Optical Transitions from Hexavalent Chromium in Lithium-Borate Glasses

Dhia-Aldin Slibi
Al-Azhar University Faculty of Science
Moukhtar Hassan (moukhtar_hassan@yahoo.com)
Al-Azhar University Faculty of Science https://orcid.org/0000-0002-5907-0295
Zakaria M. Abd El-Fattah
Al-Azhar University Faculty of Science
M. Atallah
Higher Technical Institute, 10th of Ramadan City
M. A. El-Sherbiny
Al-Azhar University Faculty of Science
M. Farouk
Al-Azhar University Faculty of Science

Research Article

Keywords: Chromium hexavalent/trivalent, Borate glasses, Colored glasses, UV-Visible optical devices, ESR

Posted Date: April 13th, 2021

DOI: https://doi.org/10.21203/rs.3.rs-307888/v1

Version of Record: A version of this preprint was published at Optical and Quantum Electronics on August 14th, 2021. See the published version at https://doi.org/10.1007/s11082-021-03147-9.

Optical Transitions from Hexavalent Chromium in Lithium-Borate Glasses

Dhia-Aldin Slibi[1], Moukhtar A. Hassan[1*], Zakaria M. Abd El-Fattah[1], M. Atallah[2], M. A. El-Sherbiny[1], M. Farouk[1*]

[1]Physics Department, Faculty of Science, Al-Azhar University, Cairo 11884, Egypt

[2]Basic Science Department, Higher Technological Institute, 10th of Ramadan City, Egypt

Abstract:

The melt-quenching technique was used to prepare a series of chromium-doped borate glasses with the composition $x Cr_2O_3$ - (70-x) B_2O_3- 30 Li_2O- (x = 0, 0.1, 0.2, 0.3 and 0.5 mol %). The low-doping level here employed allowed to unambiguously identify well-defined near-edge Cr^{6+} optical transitions, and to precisely determine the optical band gap of the borate glass host. Additional Cr^{3+} transitions were observed in the visible regime, rendering a strong modulation of the glass color, from colorless to dark greenish, with Cr content. Both Cr^{6+}(after the charge transfer transformation into Cr^{5+}) and Cr^{3+}oxidation states and their variations with Cr doping were identified from electron spin resonance spectroscopy. All samples exhibit similar vibrational spectra dominated by BO_3 and BO_4 structural units, with the development of weak Cr^{6+} vibration with Cr doping. The present study provides structurally similar but optically active and tunable glass hosts suitable for various optical applications.

Keywords: *Chromium hexavalent /trivalent; Borate glasses; Colored glasses; UV-Visible optical devices; ESR.*

---

* moukhtar_hassan@yahoo.com; m.a.hassan@azhar.edu.eg (Moukhtar A. Hassan)
* mf_egypt22375@yahoo.com; m_farouk@azhar.edu.eg (M. Farouk)

1. Introduction

Colored glasses acquired a lot of interest in commercial business as they are favored in home decoration and many other technological applications. Optical transitions between energy split *d* and *f* levels in transition metals (TM) and rare earth ions, respectively, are the main origin for color effects [1-10]. For precise and controlled tunability of glasses color, for example, it is appealing to search for suitable glass hosts capable of accommodating varies concentrations of TM ions. For this purpose, alkali borate glasses are convenient host given its low cost, transparency, and chemical/thermal stability [9-13]. Most importantly, alkali-borate glasses act as efficient TM hosts, since they offer two distinct structural units (BO_3 or BO_4), in addition to their possible conversion when doped with alkali oxides [10-13].Chromium is a TM ion that offers different oxidation states (such as Cr^{3+}, being the most stable, $Cr^{4+,}$ Cr^{5+} and Cr^{6+}) playing different rules (former or modifier) in glassy matrix depending on its valence state [2]. Low level doping of chromium ions in glasses causes color effects, the degree of which depend on its concentration. Moreover, Cr^{3+}ions have significant sensitivity to possible structural changes that affect the optical and magnetic properties [14]. The random structure of glasses renders different environment for each Cr^{3+} ion as a consequence of differences in bonding to nearest-neighbor ions. This results in site-to-site variations in the energy level structure and, consequently, to radiative and non radiative transition probabilities of Cr^{3+} ions in glasses [15]. Therefore, the optical absorption spectra will be a convolution of cooperating individual crystal-field sites.

In this study, the optical absorption and electron spin resonance (ESR) spectroscopes were used to probe the optically active Cr^{6+} and Cr^{3+} optical transitions for different Cr content. The lowest doping level here explored allows to clearly resolve the discrepancies reported for the correct estimation of the band edge in the presence of Cr^{6+} transitions.

2. Experimental

The selected glassy compositions$x$$Cr_2O_3$ - (70-x) B_2O_3- 30 Li_2O- (x = 0, 0.1, 0.2, 0.3 and 0.5 mol %) were prepared by conventional melt quenching technique. Appropriate quantities of chemicals [Cr_2O_3, B_2O_3, and LiO_2] were weighted according to their molar rations, mixed, and grinded finely in an agate mortar to achieve high homogeneity of reactants. The batches were placed in porcelain crucibles and eventually melted in an electrical furnace at 950 ^oC for 1 h. The melts were taken out after 30min of heating

process and packed into furnace for additional 30min. In order to fabricate bubbles-free glass pellets, the melts were quenched in air between two well-polished copper plates at room temperature. The chromium-free sample was found to be colorless, while other samples became greener with increasing Cr content. Fourier transform infrared absorption spectra were obtained at room temperature using FTIR (Perkin Elmer) spectrophotometer in the range 2200–400 cm^{-1}. The samples were grinded, and the resulting powders were thoroughly mixed with high purity KBr. Optical absorption spectra of all glasses were carried out using UV–VIS spectrophotometer (JenWay-6405 UV–VIS Spectrophotometer) in the range 200–1000 nm. ESR spectra were recorded using an EMX-Bruker operating in X-band frequency, and having 100 kHz field modulation. The power of the used microwave was 10 mW, and a fixed amount of glass powder from each sample was inserted in a quartz tube, while the magnetic field was scanned in the range 75-5000 G.

3. Results and discussion

3.1. Optical Absorption Results

The optical absorption spectra for all glass systems are given in Fig. 1. The spectrum of Cr-free (*i.e.*, $x = 0$) sample is featureless, except for a well-defined absorption edge at ~ 3.57 eV (black arrow) defining the band gap energy of the host. A first insight into the optical absorption spectra of Cr-doped samples reveals remarkable changes of the energetic position of the absorption edge. In particular, for the maximum doping level here used (*i.e.*, sample with $x = 0.5$), the apparent absorption edge could mislead the estimation of the band gap to be ~ 2.6 eV. Notice that a ~ 1 eV change in the band edge for such a tinny Cr-doping ($x = 0.5$) is unpredictable, although earlier borate-related literature reported underestimated energy gaps within the range 2-2.5 eV [16-23]. In fact, such large underestimation of band edge position and gap size is also found for other glassy systems [24-28] and TM-doped semiconductor nano materials [29-32]. In order to shed the light on the fine near-edge details, lower Cr-doping levels ($x< 0.5$) are used. The spectra of these slightly doped systems exhibit distinguishable near-edge absorption peaks, which lie at the origin of such misleading edge assignment. In fact, these absorption features (red arrows) are brought by Cr^{6+} characteristic optical transitions commonly found at ~ 338 and ~ 370 nm, and are assigned to $^4A_{2g} \rightarrow {}^4T_{1g}$ and to $^4A_{2g} \rightarrow {}^2A_{1g}$ transition, respectively [1-4,33-37]. Actually, Cr^{6+} is optically inactive since it has $3d^0$ configuration, but the charge transfer taking place between O and Cr ions leads to the optically active Cr^{5+} ($3d^1\ 2p^5$) state [1-3,38-41]. The intensity of Cr^{6+}

peaks clearly gains more intensity with Cr-doping, until a saturation in the UV region is achieved for the $x = 0.5$ sample. These findings allow concluding that the apparent huge shift of optical band edge results from the dominant Cr^{6+} spectral features in this regime. Additionally, both the absorption edge and Cr^{6+} peaks experience a slight red shift [1-3].

In the visible regime, Cr^{3+}ions feature two additional optical transitions (blue arrows)which are responsible for the glass color [42]. These bands located at ~421 nm and ~619 nm (as shown in Fig. 1) define the yellow and greenish colors, respectively. The bands originate from Cr^{3+} ions *d-d* transitions in octahedral environment, and are assigned to $^4A_{2g} \rightarrow {}^4T_{1g}$ and $^4A_{2g} \rightarrow {}^4T_{2g}$ transitions, respectively [1-3,33-46]. These peaks systematically gain intensity and undergo a slight red shift with increasing Cr_2O_3 content, thereby changing the glass color from colorless to dark greenish as shown at the inset of Fig. 1.

The crystal field parameters, such as crystal field strength (10Dq) and Racah parameters (B &C) can be deduced from the following equations: [1-3,33-37];

$$10Dq = \upsilon_1 \tag{1}$$

$$B = \frac{(2\upsilon_1 - \upsilon_2)(\upsilon_2 - \upsilon_1)}{(27\upsilon_1 - 15\upsilon_2)} \tag{2}$$

$$C = \frac{\upsilon_3 - 4B - \upsilon_1}{3} \tag{3}$$

where υ_1, υ_2 and υ_3 refer, respectively, to the bands positioned at 619 nm (Cr^{3+}) , 421 nm (Cr^{3+}) and the average sum of 337 and 369 bands (Cr^{6+}) all taken in cm^{-1} energy units. Fig. 2 presents these legend field parameters as a function of Cr_2O_3 content. It is noticed that the value of 10Dq (B and C) increases (decreases) with introducing more Cr ions, indicating weaker *d* shell inter-electronic repulsion.

The ratio between Racah parameters (C/B) was found to be~ 3.8 as listed in Table 1. Likewise, the ratio Dq/B is found to increase from 2.13to 2.38 indicating a crossover from the weak to moderate crystal field with Cr_2O_3 content [1-3,18]. The estimated bond formation represented as the nephelauxetic parameter (h) is given as [1-3,18,25]:

$$h = \frac{[(B_{free} - B)/B_{free}]}{K_{Cr^{3+}}} \tag{4}$$

where B_{free} defines the Racah parameter for gaseous Cr^{3+}, and K_{Cr3+} is the central Cr^{3+} ion, which take the values B_{free}= 918 cm^{-1} and K_{Cr3+}= 0.21 [1-3,25,36]. Therefore, for

all glass samples, B is lower than B_{free}, as given in Table 1. The estimated *h* parameter increases with Cr_2O_3 content, indicating more covalent environment for Cr^{3+}ions and increased *d*-electrons localization [1,25,36].

3.2. FTIR RESULTS

Fig.3 presents the FTIR spectra of all glass samples, while the corresponding peak assignments and energetic positions for the various fundamental vibrational units of borate and chromium networks are listed in Table 2.To obtain precise information about structural changes within the glass a detailed deconvolution process, using a number of Gaussian bands, is required. The structure of borate glasses consists of a random network of planar triangles BO_3 with a certain fraction of six-member rings [1-3,25,39]. The addition of alkali oxides as a modifier transforms some of BO_3 into four coordinated tetrahedral BO_4 units [47]. All spectra showed three, but rather broad, main bands characteristic for planar triangles BO_3 with a certain fraction of six-member rings [39,25] and four coordinated tetrahedral BO_4 units [47] commonly found for alkali borate glasses. Such broadening is most likely due to the combination of highly degenerate vibrational states, thermal broadening of the lattice dispersion band, and mechanical scattering from powder samples. The first band (shaded in blue) ranged from 1600 to 1170 cm^{-1}(centered at 1360 cm^{-1}) is correlated to the stretching vibrations of B-O-B bond in the trigonal BO_3 unit [18,20,21,48].This band revealed a clear splitting into three separate features at ~1233 cm^{-1} and (~1330 & 1415 cm^{-1}), which are due to the existence of two types of BO_3 units containing non-bridging oxygen (NBO) atoms at blue arrow and those connected to the glass network by all three oxygen atoms (free of NBO), respectively [2].The NBO was found to slightly increase with Cr_2O_3 content. The recorded band at ~1500 cm^{-1} is attributed to overlap between the triangles and the O-H bending vibration mode **[**18,20**]**. The second main broad band (shaded in yellow) observed within the range 1170 – 780 $cm^{-1}$is attributed to B-O and B-O-B stretching and rocking motions associated with BO_4[18,20,21,48]. Likewise, the band splits into three features at ~870 cm^{-1} and (~940 & 1050 cm^{-1}), in correlation with BO_4 units connected to barely affected NBO (black arrow) and to all four oxygen atoms, respectively [2]. The third band (shaded in blue) located in the region 780-590 cm^{-1}, with center at 690 cm^{-1}, is attributed to the bending mode of long chain structural unit of $(B_3O_7)^{5-}$ species [18,20,21,48-50], i.e. boron atoms vibrate perpendicular to O_3 plane of their triangles BO_3. On the other hand, a weak feature is observed at ~540 cm^{-1} which belongs to the B–O–B vibrations and/or borate ring deformations [2,51,52]. Below 500

cm^{-1} a band of Li ionic vibration is observed [1-3,53]. Finally, samples containing higher Cr concentration (*e.g.*, x = 0.3, 0.5 mol%), exhibit weak feature at ~ 470cm^{-1} which belongs to vibrations of Cr^{6+} in Cr_4^{2-} structural units[1,2,27,54].These fine features are easily seen in the zoom-in and deconvoluted spectra presented in Fig. 4(a). The Cr and Li bands, identified after the deconvolution process, clearly increase with Cr ions concentration as depicted in Fig. 4(b). Contrarily, the value of N_4 (which quantifies the relative population of borate species) decreases from 46 % to 38% with the concentration of C_2O_3, while the NBOs are barely increased.

3.3. ESR Results

ESR spectra for 0.1, 0.2, 0.3 and 0.4 Cr-doped samples are presented in Fig. 5. The spectra were all normalized with respect to their mass to ensure a reasonable quantitative comparison. As evident from Fig.5, there exist four resonances with effective g values 4.9 and 4.1, at low field, and 2.2 and 1.9, at high field. The two low field resonances with g = 4.9 and 4.1 are vastly reported to originate from isolated Cr^{3+} ion sites of rhombic symmetry exposed to strong ligand field [1-3,34,36,47,45,55,56]. The resonance signal observed at the effective value of g = 2.2-2.3 has been attributed to exchange coupled pairs of Cr^{3+-} Cr^{3+} ions [34,37,45]. The sharp resonance signal with effective g = 1.9 most likely arises due to Cr^{5+} ions (*i.e.*, the charge transfer state of Cr^{6+}) [1-3,18,33,40]. The intensity of this resonance increases, almost linearly, with increasing Cr content. However, the intensity dependence for the other three resonances on Cr concentration has non-monotonic behavior. The two low field resonances with effective g values g= 4.9 and 4.1 follow quite similar behavior with Cr concentration, which indicates that the two signals have the same origin (i.e., Cr^{3+} ions).The 0.3 Cr sample exhibits the strongest intensity deviation among this doping series, where the resonance for g= 2.2-2.3 is the most intense (shaded region) while the intensity for the other two low field signals at g= 4.9 and 4.1 are lowered. This may be attributed to the presence of large fraction of Cr^{3+} ions exchange coupled in pairs for this sample. In fact, by considering the overall area under all Cr^{3+} resonance, *i.e.*, the two low field (g = 4.9 and 4.1) and the high field (g = 2.2-2.3) resonances, the average Cr^{3+} contributions increases monotonically with Cr concentration.

Conclusion:

Chromium-doped borate glass systems of composition $x$$Cr_2O_3$ - (70-x) B_2O_3- 30 Li_2O_3 with exceedingly small doping level (x = 0, 0.1, 0.2, 0.3 and 0.5 mol %) were prepared utilizing the melt quenching technique. For such a diluted Cr-doping, well-defined near-

edge Cr^{6+} optical transitions were unambiguously identified, and the optical band gap of the glass systems was precisely determined. Away from the absorption edge, specifically in the visible spectral regime, additional Cr^{3+} transitions showed up thereby modulating the glass color from colorless to dark greenish with increasing Cr content. The existence of both Cr^{6+} and $Cr^{3+}$was ensured by measuring their oxidation states using electron spin resonance spectroscopy. The vibrational spectra for all samples were similarly dominated by borate characteristic groups, namely BO_3 and BO_4 structural units, while additional weak Cr^{6+} vibrations are developed with Cr doping.

References

1) M.A. Hassan, F. Ahmad, Z.M. Abd El-Fattah, J. Alloys Compd. 750 (2018) 320.
2) Moukhtar A. Hassan, F.M. Ebrahim, M.G. Moustafa, Z.M. Abd El-Fattah, M.M. El-Okr, J. Non-Cryst. Solids 515 (2019) 157.
3) F. Ahmad, E. Nabhan, Optical and Quantum Electronics 51,8 (2019) 261
4) Hongli Wen, Peter A. Tanner, J. Alloys Compd. 625 (2015) 328.
5) Jia-Jun He, Shao-YiWu, Li-Juan Zhang, Yong-Qiang Xu, Chang-Chun Ding, J. Non-Cryst. Solids 437 (2016) 58.
6) A. Dahshan, Yasser B. Saddeek, K.A. Aly, K.H.S. Shaaban, Modather F. Hussein, Ahmed O. Abo El Naga, S.A. Shaban, S.O. Mahmoud, J. Non-Cryst. Solids 508 (2019) 51.
7) Z. M. Abd El-Fattah, F. Ahmad, M. A. Hassan, J. Alloys Compd. 728 (2017)773.
8) A. Samir, Moukhtar A. Hassan, A. Abokhadra, L. I. Soliman, M. Elokr, Optical and Quantum Electronics 51 (2019) 123.
9) M. A. Hassan, M. Farouk, I. Kashef, A.H. Abullah, M. M. ElOkr, J. Alloys Compd. 539 (2012) 233.
10) Hongli Wen, Peter A. Tanner, Bing-Ming Cheng, Mater. Res. Bull. 83 (2016) 400.
11) G. Venkateswara Rao, N. Veeraiah, J. Alloys Compd. 339 (2002) 54.
12) A.Terczyńska-Madej, K. Cholewa-Kowalska, M. Łaczka, Opt. Mater. 33 (2011) 1984.
13) W.A. Pisarski, J. Pisarska, G. Dominiak-Dzik, W. Ryba-Romanowski, J. Alloys Compd. 484 (2009) 45.
14) M. Farouk, D-A. Slibi, Z. M. Abd El-Fattah, M. Atallah, M. A. El-Sherbiny, and Moukhtar A. Hassan, Silicon (2021) https://doi.org/10.1007/s12633-020-00649-1
15) K. K. Chattrjee and L. S. Forster, Spectrochimica Acta 20 (1964) 1603.

16) A.R. Molla, C.R. Kesavulu, R.P.S. Chakradhar, A. Tarafder, S.K. Mohanty, J.L. Rao, B. Karmakar, S.K. Biswas, J. Alloys Compd. 583 (2014) 498.
17) F. Ahmad, J. Alloys Compd. 586 (2014) 605.
18) C.R. Kesavulu, R.P.S. Chakradhar, C.K. Jayasankar, J. Lakshmana Rao, J. Mol. Struct. 975 (2010) 93.
19) M.A. Hassan, J. Alloys Compd. 574 (2013) 391.
20) G. Naga Raju, N. Veeraiah, G. Nagarjuna, P.V.V. Satyanarayana, Phys. B 373 (2006) 297.
21) F.H. ElBatal, Y.M. Hamdy, S.Y. Marzouk, J. Non-Cryst. Solids 355 (2009) 2439.
22) H.A. El Batal, E.M. Abou Hussein, N.A. El Alaily, F.M. EzzEldin, J. Non-Cryst. Solids 528 (2020) 119733.
23) O. I. Sallam1 · F. M. Ezz-Eldin1 · N. A. Elalaily, Optical and Quantum Electronics 52 (2020) 204.
24) B. Lakshmana Rao, Y.N.Ch. Ravi.Babu, S.V.G.V.A. Prasad, J. Non-Cryst. Solids 382 (2013) 99.
25) F. S. De Vicente, F.A. Santos, B.S. Simões, S.T. Dias d, M. Siu Li, Opt. Mater. 38 (2014) 119.
26) R. Vijay, P.Ramesh Babu, V. Ravi Kumar, M. Piasecki, D. Krishna Rao, N. Veeraiah, Mater. Sci. Semicond. Process. 35 (2015) 96.
27) T. Narendrudu, S. Suresh, G. Chinna Ram, N. Veeraiah, D. Krishna Rao, J. Lumin.183 (2017) 17.
28) M.V. Sambasiva Rao, Ch. Rajyasree, T. Narendrudu, S. Suresh, A. Suneel Kumar, N. Veeraiah, D. Krishna Rao, Opt. Mater. 47 (2015) 315.
29) I. Y. Habib, A. A. Tajuddin, H. A. Noor, C. M. Lim, A. H. Mahadi, and N. T. R. N. Kumara, Sci. Rep. 9 (2019) 9207.
30) R. S. Dubey, S. Singh, Results Phys. 7 (2017) 1283.
31) V. R. Akshay, B. Arun, G. Mandalc, and M. Vasundhara, Phys. Chem. Chem. Phys. 21 (2019) 12991.
32) V. Dattu Mote, V. R. Huse, and B. N. Dole, World J. Condens. Matter Phys. 2 (2012) 208.
33) A. Terczynska-Madej, K. Cholewa-Kowalska, M. Laczka, Opt. Mater. 32 (2010) 1456.
34) B.V. Padlyak, W. Ryba-Romanowski, R. Lisiecki, V.T. Adamiv, Ya. V. Burak, I.M. Teslyuk, Opt. Mater. 34 (2012) 2112.

35) R.V.S.S.N. Ravikumar, R. Komatsu, K. Ikeda, A.V. Chandrasekhar, B.J. Reddy, Y.P. Reddy, P.S. Rao, J. Phys. Chem. Solids 64 (2003) 261.
36) R.V.S.S.N. Ravikumar, J. Yamauchi, A.V. Chandrasekhar,Y.P. Reddy, P. Sambasiva Rao, J. Mol. Struct.740 (2005) 169.
37) Vijay Singh, G. Sivaramaiah, J.L. Rao, S.H. Kim, Mater. Res. Bull. 60 (2014) 397.
38) Cz. Koepke, K. Wiśniewski, M. Grinberg, J. Alloys Compd. 341 (2002) 19.
39) Cz. Koepke, K. Wiśniewski, M. Grinberg, F. Rozpłoch, J. Phys.: Condens. Matter 14 (2002) 11553.
40) G. Little Flower, M. Srinivasa Reddy, G. Sahaya Baskaran, N. Veeraiah, Opt. Mater. 30 (2007) 357.
41) G. Murali Krishna, B. Anila Kumari, M. Srinivasa Reddy, N. Veeraiah, J. Solid State Chem.180 (2007) 2747.
42) Olfa Taktak, Hajer Souissi, Kammoun Souha, Journal of Luminescence 161 (2015) 368.
43) J. Lakshmana Rao, B. Sreedhar, M. Ramachandra Reddy S.V.J. Lakshman. J. Non-Cryst. Solids 111 (1989) 228.
44) D.K. Durga, N. Veeraiah, Phys. B 324 (2002) 127.
45) Vijay Singh, R.P.S. Chakradhar, J.L. Rao, Ho-Young Kwak. Solid State Sciences 11 (2009) 870.
46) G. Giridhar, S.Sreehari Sastry, M.Rangacharyulu, Phys. B 406 (2011) 4027.
47) A.K. Varshneya, Fundamentals of Inorganic Glasses, Academic press Inc, New York, 1994.
48) Subhashini, H.D. Shashikala, N.K. Udayashankar, J. Alloys Compd. 658 (2016) 996.
49) S. Suresh, T. Narendrudu, S. Yusub, A. Suneel Kumar, V. Ravi Kumar, N. Veeraiah, D. Krishna Rao, Spectrochim. Acta A Mol. Biomol. Spectrosc. 153 (2016) 281.
50) Mahesh M. Hivrekar, D. B.Sable, M.B. Solunke, K.M. Jadhav, J. Non-Cryst. Solids 474 (2017) 58.
51) M.G. Moustafa, M.Y. Hassaan, J. Alloys Compd. 710 (2017) 312.
52) N.C.A. de Sousa, M.T. de Araujo, C. Jacinto, M.V.D. Vermelho, N.O. Dantas, C.C. Santos, I. Guedes, J. Solid State Chem. 184 (2011) 3062.
53) M. Vijayakumar, K. Marimuthu, V. Sudarsan. J. Alloys Compd. 647 (2015) 209.

54) Parminder Kaur, K.J. Singh, Murat Kurudirek, Sonika Thakur, Spectrochim. Acta A Mol. Biomol. Spectrosc.223 (2019) 117309.
55) H. Schneider, K. Ikeda, B. Saruhan, H. Rager, J. Eur. Ceram. Soc. 16 (1996) 211.
56) C. Laxmi Kanth, B.V. Raghavaiah, B. Appa Rao, N. Veeraiah, J. Quant. Spectrosc. Radiat. Transf. 90 (2005) 97.

Table 1: Band gap energy and Ligand field parameters (C/B & Dq/B ratios and neplequestic parameter).

Cr_2O_3 content (mol. %)	Band gap energy	Ligand field parameters		
	E_g (eV)	C/B	Dq/B	*h*
0.0	3.57	-	-	-
0.1	3.56	3.77	2.13	0.804
0.2	3.52	3.80	2.24	0.962
0.3	3.49	3.83	2.29	1.046
0.5	3.37	3.79	2.38	1.177

Table 2: Assignment of FTIR vibrational bands present in all glassy samples.

Spectral region in (cm^{-1})	*Assignment*	*Ref.*
1150-1600	Asymmetric stretching vibrations of triangle BO_3	[18,20,21,50]
1500	Overlap with the triangles band due to the O–H bending vibration mode	[18,20]
780-1170	B–O rocking and stretching motion in BO_4 tetrahedral	[18,20,21,50]
590-780	B–O–B symmetric bending of triangle vibrations.	[18,20,21,50]
540	B–O–B vibrations	[2,48,49]
470	Cr-O in hexavalent state which is a network former with CrO_4^{2-} form	[1,2,27,54]
Below 500	Li ion vibration	[1-3,53]

Figures

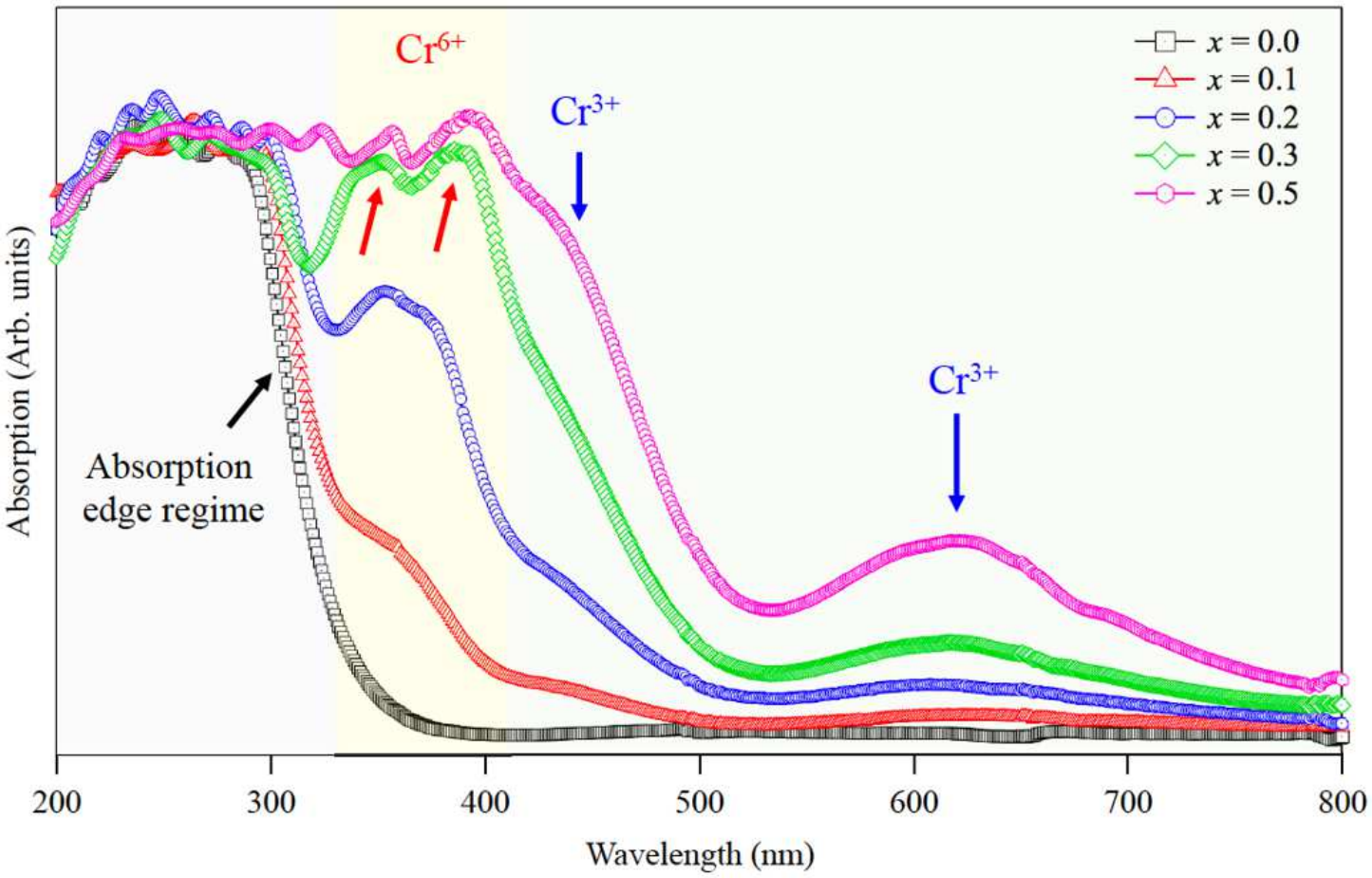

Figure 1

Optical absorption spectra for all glassy samples. The black, red, and blue arrows define the position of the absorption edge, Cr6+, and Cr3+ transitions, respectively. The thick white-green arrow and samples photos highlight the fine changes in the glass color with Cr-doping.

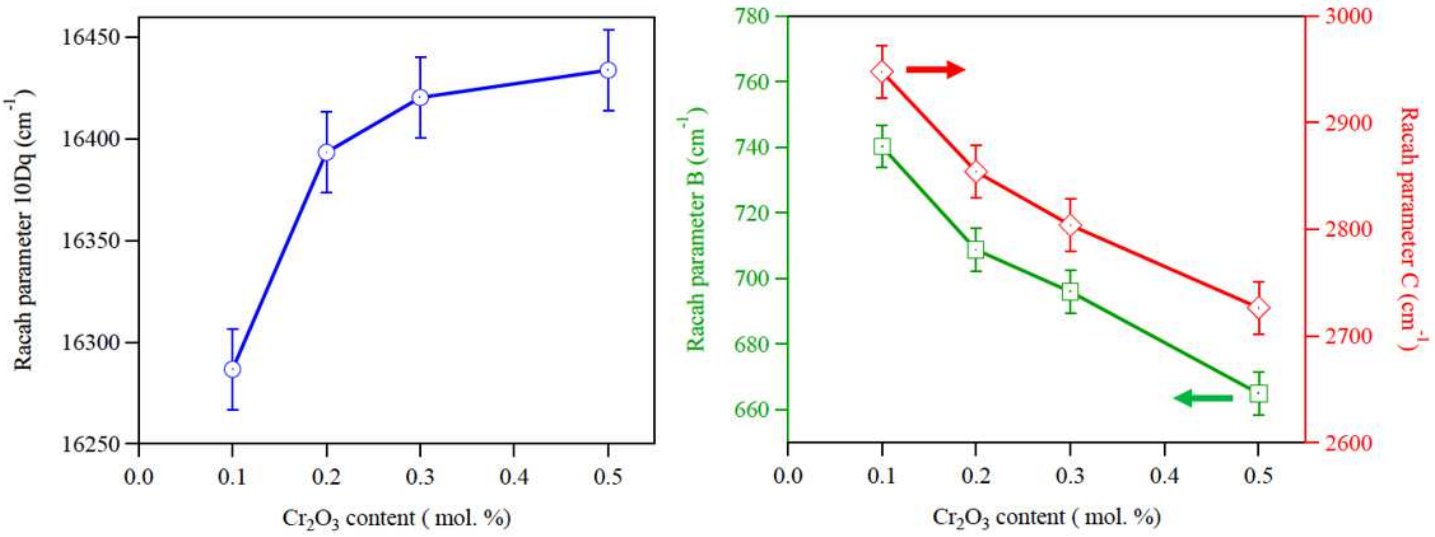

Figure 2

Composition dependence of Ligand field parameters, namely (left) crystal field strength (10Dq) and (right) Racah parameters (B,C).

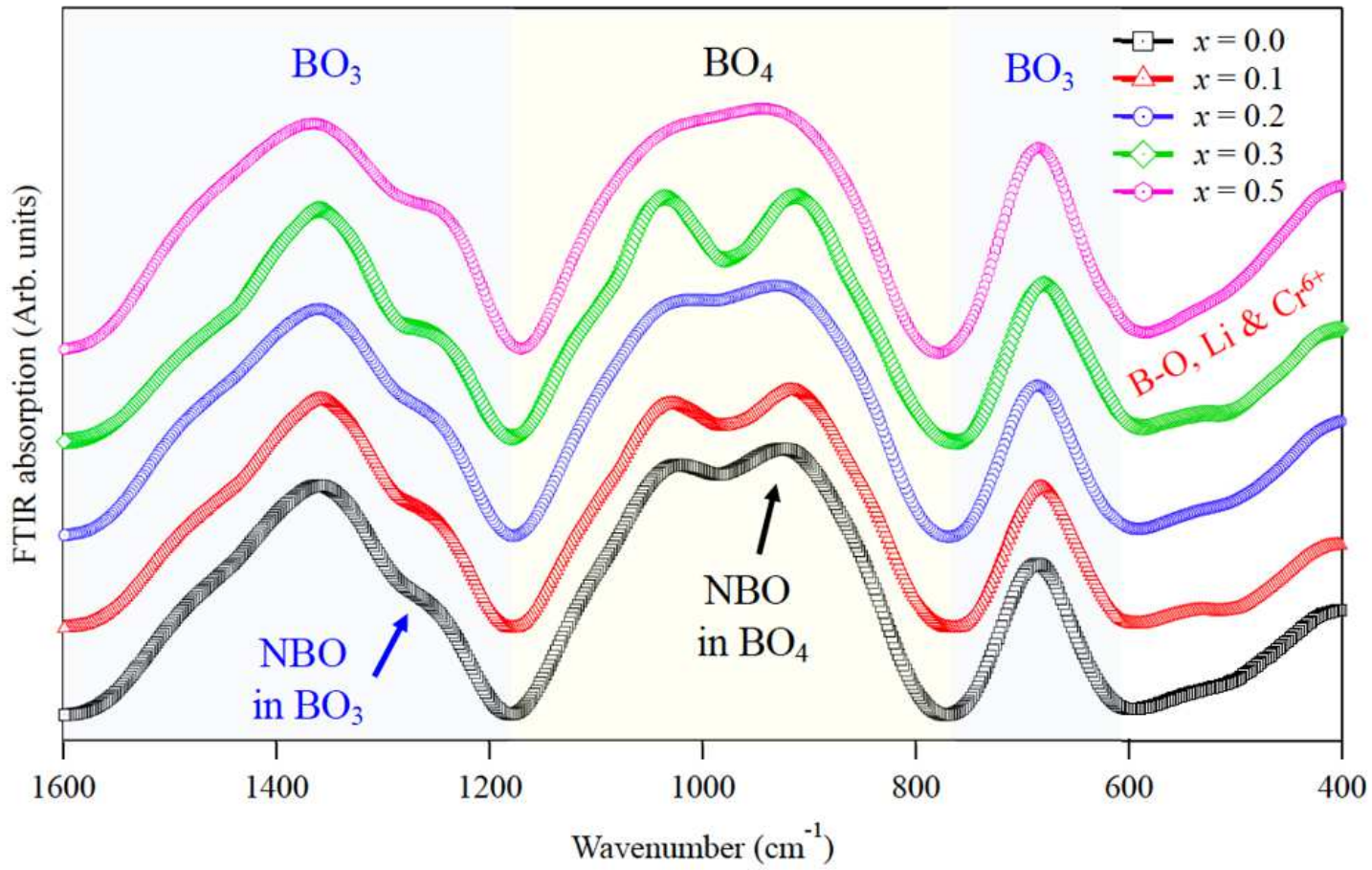

Figure 3

FTIR spectra of all prepared samples. The blue and yellow shaded areas correspond to vibrations from BO3 and BO4 structural units, respectively. The arrows indicate the peak position of NBO.

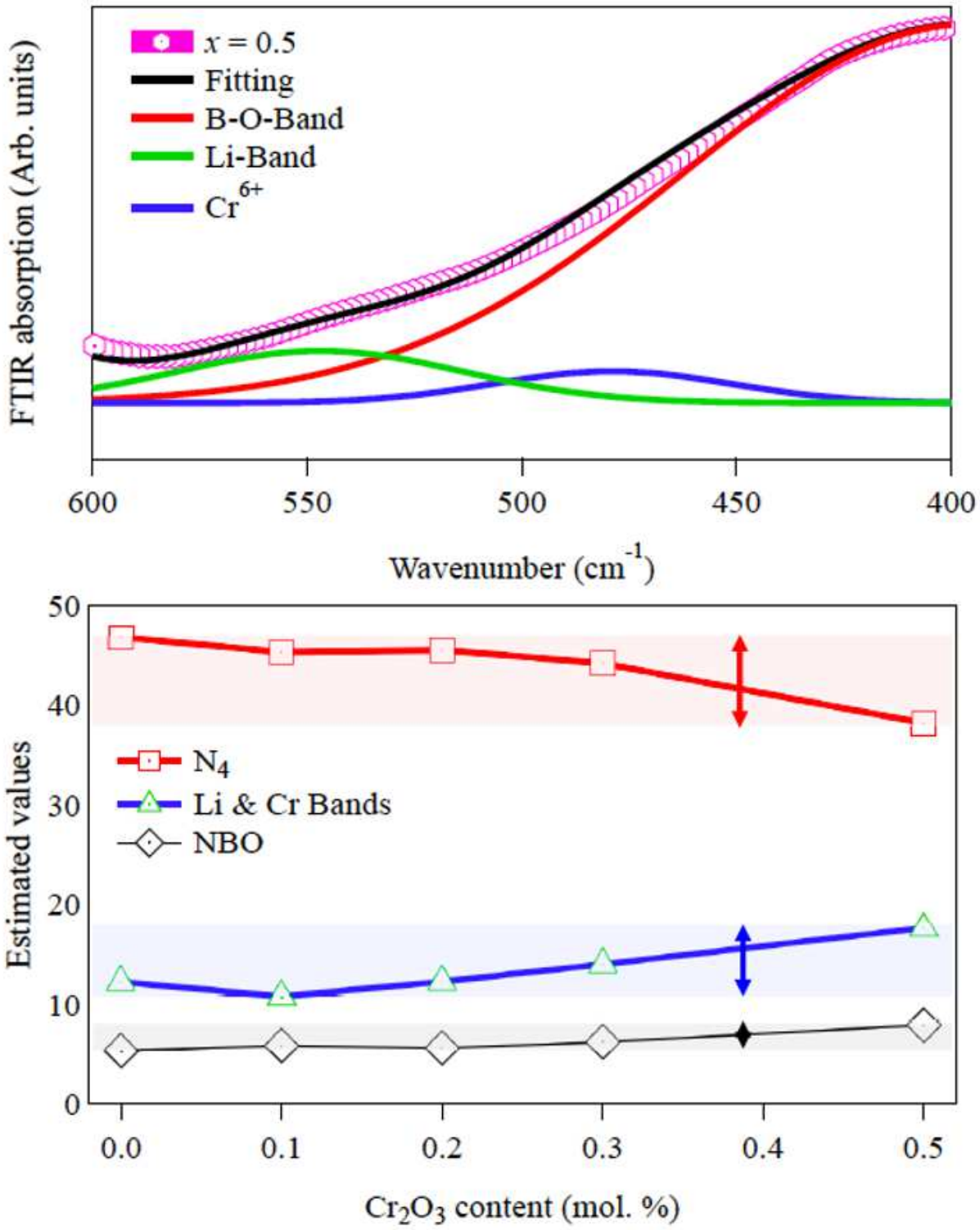

Figure 4

(Top) Deconvolution process for the x = 0.5 samples, in the low wavenumber side, showing Cr6+, Li, and B-O-B vibrations. (Bottom) Variation of N4, NBO, and Li&Cr bands as a function of Cr2O3 content. The length of the vertical arrows highlights the maximum observed change.

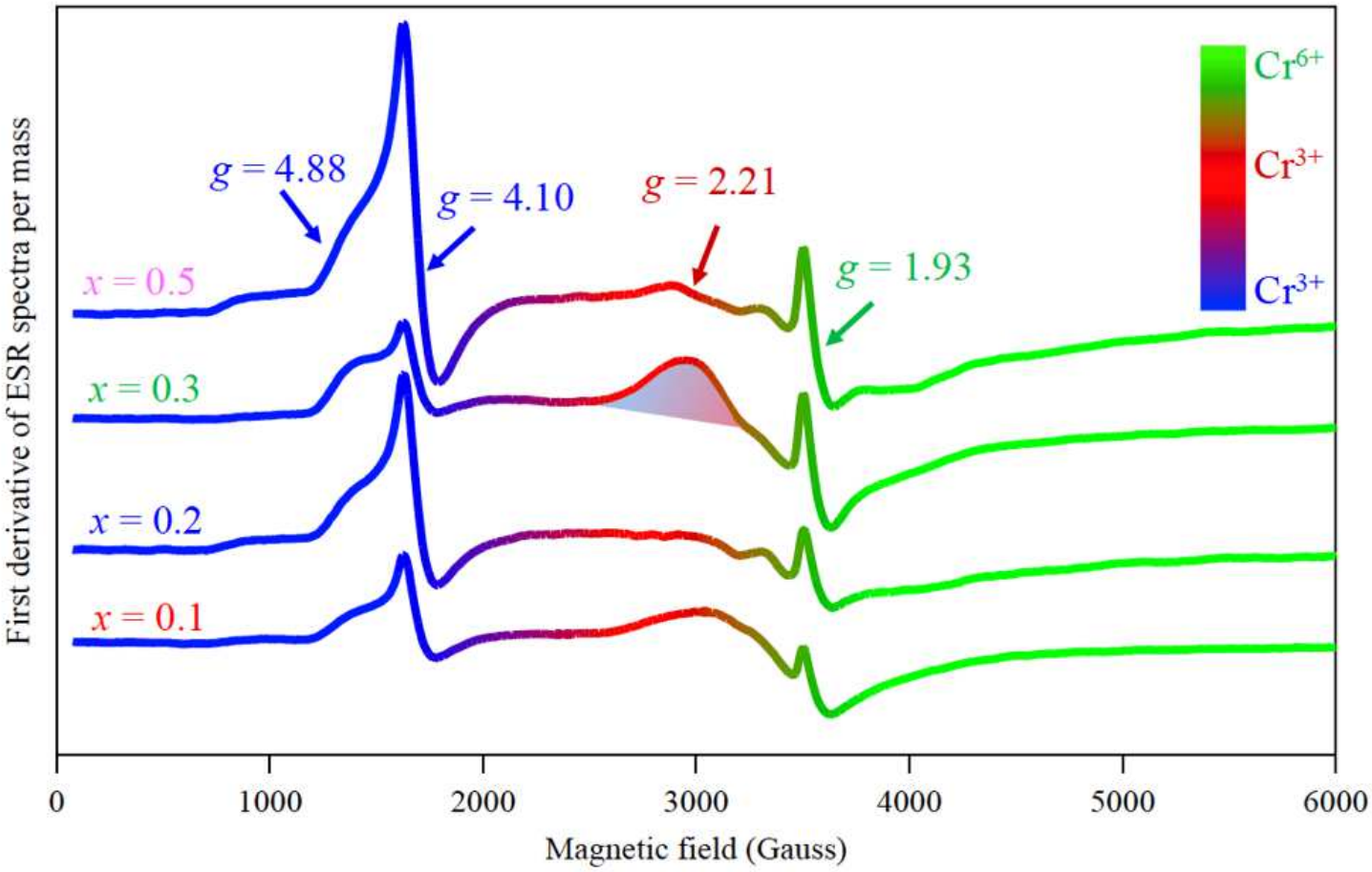

Figure 5

ESR spectra for all chromium doped samples. The color scale distinguishes resonance from Cr3+(blue-red) and Cr6+ (green) oxidation states.